Open Access Library Journal
2023, Volume 10, e9875
ISSN Online: 2333-9721
ISSN Print: 2333-9705

HAP/f-MWCNTs/Cobalt Ferrites Nano Composites Synthesis and Electrical and Magnetic Performance Investigation

Mohammad Mostafa Raja[1], Rabiul Awal[1,2*], Jahirul Islam Khandaker[1], Mohammad Al-Mamun[3], Mohammad Mahbubul Haque[3], Nilufer Yesmin Tanisa[1,2], Mohammad Sheikh Farid[2], Sayed Muhammad Shahid Hasan[2], Shamima Meherin[2]

[1]Department of Physics, Jahangirnagar University, Dhaka, Bangladesh
[2]Department of Physics, Uttara University, Dhaka, Bangladesh
[3]Materials Science Division, Atomic Energy Centre, Dhaka, Bangladesh
Email: *rabiulnanophy@gmail.com

How to cite this paper: Raja, M.M., Awal, R., Khandaker, J.I., Al-Mamun, M., Haque, M.M., Tanisa, N.Y., Farid, M.S., Hasan, S.M.S. and Meherin, S. (2023) HAP/f-MWCNTs/Cobalt Ferrites Nano Composites Synthesis and Electrical and Magnetic Performance Investigation. *Open Access Library Journal*, **10**: e9875.
https://doi.org/10.4236/oalib.1109875

Received: February 15, 2023
Accepted: March 28, 2023
Published: March 31, 2023

Abstract

In the current study, pristine multiwalled carbon nanotubes (p-MWCNTs) were functionalized by HNO_3 for introducing carboxyl functional group on the MWCNTs surface by which hydroxyapatite (HAP) molecules were grafted onto the surface of functionalized multiwalled carbon nanotubes (f-MWCNTs) with strong interfacial bonding. HAP-fMWCNTs-Cobalt ferrite composites were synthesized successfully by the homogenous mixture method. XRD analysis revealed that crystalline peaks of the HAP-f-MWCNTs-Cobalt ferrite composites were sharper than that of the pure HAP, f-MWCNTs, and cobalt ferrite which indicated that crystalline phases of HAP and cobalt ferrite on f-MWCNTs sidewall possessed high crystallinity. FTIR spectra of the composites sintered at 800˚C confirmed the f-MWCNTs and ferrite along with HAP. But dielectric constant was decreased with increasing frequency. The dielectric constant depended upon the polarizability of the materials. The dielectric loss factor of the composites at the beginning was very high but started to decrease immediately with increasing frequency. VSM data identified that HAP/3% f-MWCNTs/$5CoFe_2O_4$ composite was a highly magnetic material as it processed the highest coercivity of 850.50 Oe with magnetization 2400 emu/g.

Subject Areas

Material Experiment

Keywords

Hydroxyapatite (HAP), Multiwalled Carbon Nanotubes (MWCNTs), Ferrites, Dielectric Constant, and Resistivity

1. Introduction

Considerable research has been reported in the improvement of calcium phosphate ceramics as implantation. There are many customs of calcium phosphate ceramics that are deliberated biocompatible. Because of its comparable chemical conformation and crystal structure to apatite in the human skeletal organism, hydroxyapatite [$Ca_{10}(PO_4)6(OH)_2$, (HAP)] is one of the most recognized phases researched for a variety of biological applications [1]. Other uses of HAP include protein purification, drug carrier, human eye replacement, and bone deformities in orthopaedic maxillofacial surgery and dentistry [2] [3] [4] [5]. Mechanical, optical, electrical, and magnetic properties of nano hydroxyapatite biomaterials [6] are also present. CNTs are interesting in the field of material science because of their noble mechanical qualities such as high resilience, flexibility, and tensile strength, as well as other unique structural, electrical, and physicochemical features [7] [8] [9]. Many papers are reported on the preparation and mechanical characterization of composites, its poor dissolution property restricts the application of CNTs [10]-[14]. As a result, HAP/MWCNTs composites have a wide variety of therapeutic applications [15]. As a result, if the composite is prepared using CNTs and other technical materials, the CNTs can reinforce and toughen the matrix. Some use materials can be obtained by utilizing the unique nanometre effect of CNTs. Theoretical research has demonstrated that CNTs may be used to create composites with extremely high mechanical properties. One of the most intriguing research subjects is the investigation of CNTs composites. CNT-based composites such as CNTs/metal, CNTs/ceramic, and CNTs/polymer have been developed [16] [17]. However, a few investigations on the security of CNT/ceramic composites have been published [18]. One of the bio-ceramics with the highest bioactivity is hydroxyapatite (HAP), however it has lesser mechanical properties than human load-bearing bone and requires strengthening and toughening. Cobalt ferrite ($CoFe_2O_4$) nanoparticles are one of the most studied and noteworthy magnetic nanoparticles in different spinel ferrite [19] [20]. Because of its high electromagnetic performance, outstanding chemical stability and mechanical hardness, high coercive and moderate saturation magnetization, and high coercive and moderate saturation magnetization, cobalt ferrite has received a lot of attention [21] [22]. If CNTs and HAP were combined, a composite with improved biocompatibility, greater mechanical strength, and perhaps clear magnetic and wave-absorbing capabilities may be produced [23]. We included a particular number offerrites in the CNTs/HAP composites to increase their electrical, magnetic, and catalytic capabilities.

2. Material and Methods

2.1. Materials

Calcium nitrate tetra-hydrate [$Ca(NO_3)_2 + 4H_2O$], ammonium di-hydrogen phosphate [$NH_4H_2PO_4$] and Sodium hydroxide [NaOH] were purchased from Merck KGaA, 64,271 Darmstadt, Germany. Here, chemical [$Ca(NO_3)_2 + 4H_2O$]

as Ca^{2+} source and $[NH_4H_2PO_4]$ as PO_4^{3-} source were used to synthesis of Nano-sized hydroxyapatite powder with ultrasonic precipitation method. Sodium hydroxide [NaOH] in this method was used to control the pH of the finally product hydroxyapatite powder. MWCNTs were synthesized by chemical vapor deposition (CVD) method at temperature 760˚C on quartz substrate [24]. Cobalt ferrite ($CoFe_2O_4$) nano powders were prepared by the hydrothermal method [25].

2.2. Sample Preparation

Hydroxyapatite (HAP) was synthesized by chemical precipitation method over and done with aqueous solution of the reactants $Ca(NO_3)_2 + 4H_2O]$ and $NH_4H_2PO_4$. Here NaOH solution was used as agents for pH adjustments. $[Ca(NO_3)_2 + 4H_2O]$ and $NH_4H_2PO_4$ were first dissolved and vigorously stirred in distilled water to form 1 M and 0.5 M aqueous solutions, respectively. The aqueous solution of $NH_4H_2PO_4$ was slowly added drop-wise to the $[Ca(NO_3)_2 + 4H_2O]$ solution under continuous stirring at ambient temperatures and adjusted to pH = 11 by using NaOH solution. This can be explained by the following reaction:

$$10Ca\left(NO_3\right)_2 \cdot 4H_2O + 6NH_4H_2PO_4 + 8NaOH$$
$$\rightarrow Ca_{10}\left(PO_4\right)_6\left(OH\right)_2 + 20NaNO_3 + 20H_2O$$

In the next step, the resulting solution was stirred for four hours at room temperature. The solution was aged for 24 hours to precipitation and then filtered. Then the precipitated HAP was repeatedly washed with distilled water by centrifugation method at the rotation speed of 12,000 rpm for half hour. The resulting precipitate was dried at 40˚C - 55˚C and then calcined at 100˚C, 450˚C, 900˚C, 1200˚C for one hour. The p-MWCNTs were functionalized by HNO_3 followed the method of Montoro *et al*. [26]. In a typical procedure, the p-MWCNTs (100 mg) was sonicated with concentrated HNO_3 (65%, 30 ml) in a beaker by an ultrasonic for 30 min. The dispersed suspension was boiled at 90˚C for 4 hours under reflux to gain the carboxyl functional groups (MWCNT-COOH). The dried MWCNTs was mentioned as functionalized or f-MWCNTs. Functionalized MWCNTs was dispersed in distilled water and stirred with a magnetic stirrer for 1 hours at ambient temperature. The suspensions were then homogenized in an ultrasonic bath for 30 minutes and added to ethanol to form an f-MWCNTs/ethanol slurry. The slurry was stirred for 12 hours at room temperature. After then the slurry was mixed with appropriate quantity of HAP. The resulting suspensions was shaken and stirred at 400 rpm for 2 hours. Then the suspensions were sonicated for 1 hour to obtain homogeneous mixture and left to precipitation. In the next step, the f-MWCNTs/HAP solutions were filtered and poured into a silicon cloth glass dish (8 cm × 12 cm).

The compound was then heated at 65˚C to allow water and acetone to evaporate. The dried compound with an average thickness of 0.05 mm were easily re-

moved from dish. This compound was powdered by hand milling method for 5 hours. As pre-prepared ferrites powder of different ratios was added to this powder and homogenous mixer of this composites had been done by hand milling method for 2 hours, which was HAP/MWCNTs/ferrites composites, and no particular treatment was required. Figure 1 illustrates the steps for the production of composites made of HAP, f-MWCNTs, and cobalt ferrites.

2.3. Identification Methods

For verification of the synthesis of the necessary materials, the chemical characteristics of the nanocomposites powder as it was created were examined using an IR Ptrestige-21 FT-IR (Shimadzu Europe). The physical structure and phase of the powder samples were studied by XRD (Philips X'Pert PW 3040 Powder, Baltimore, USA)Magnetic properties, such as magnetization, coercive force and hysteresis loop were studied by VSM (EV9, MicroSense, LLC, USA) analysis. Electrical properties such as frequency dependent conductivity and resistivity of the samples were investigated using impedance analyzer (6500B series, Wayne Kerr Electronics, UK).

3. Results and Discussion

3.1. XRD Analysis

3.1.1. XRD Studies of Sample HAP

XRD pattern of synthesized HAP was shown in Figure 2. Main peaks and their intensity of standard and synthesized HAP respectively was shown in Table 1.

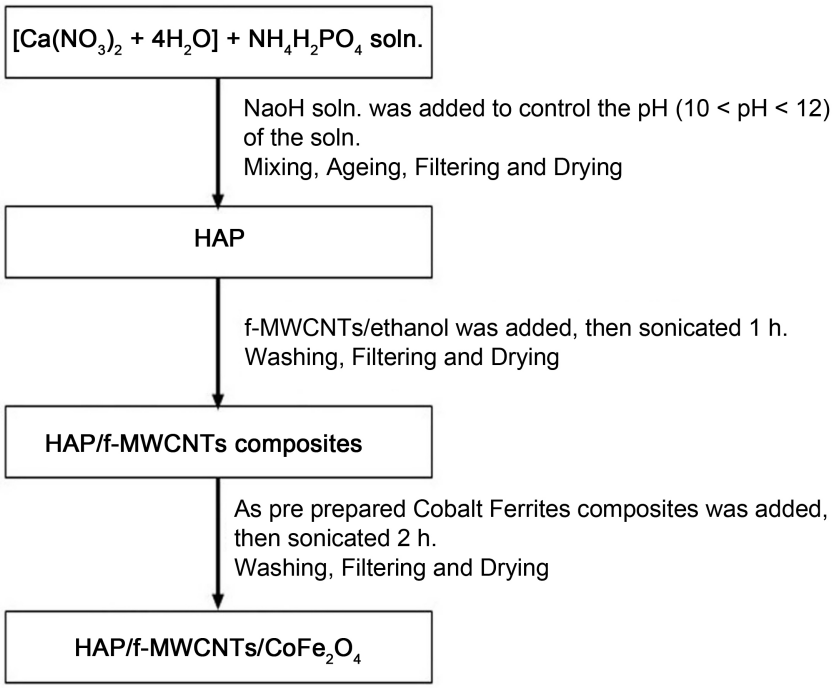

Figure 1. Illustrates the steps for the production of composites made of HAP, f-MWCNTs, and cobalt ferrites.

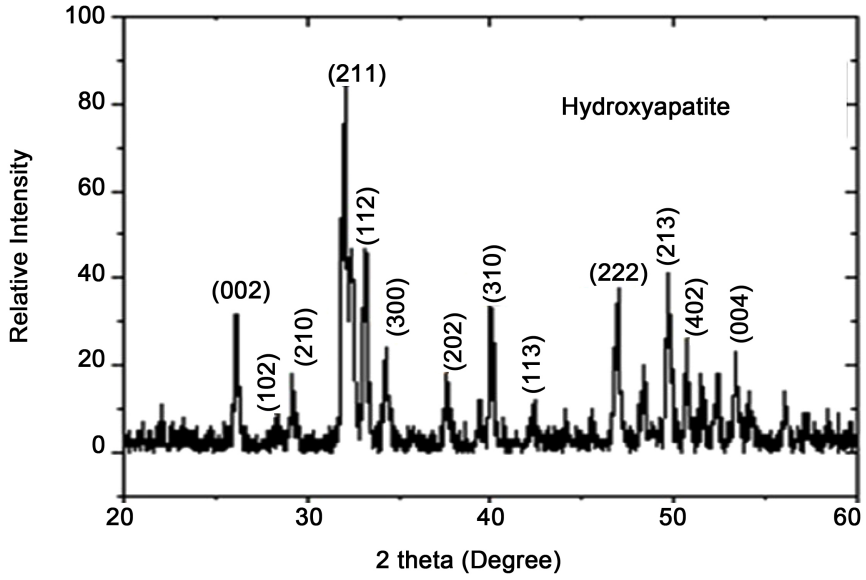

Figure 2. The XRD pattern of synthesized HAP.

Table 1. Comparison between synthesized HAP and standard HAP.

No.	Miller indices (h k l)	Hydroxyapatite			Standard Hydroxyapatite		
		d-spacing (A^0)	2θ (deg)	peak Intensity (I) %	d-spacing (A^0)	2θ (deg)	peak Intensity (I) %
1	002	3.415	26.093	31.69%	3.441	25.872	36.1
2	211	2.781	32.184	100	2.796	31.973	100
3	112	2.697	33.212	60.86	2.771	32.275	43.7
4	300	2.715	32.894	70	2.699	31.157	54.3
5	202	2.615	34.291	21.96	2.622	34.167	24.5
6	222	1.937	46.689	17.05	1.933	46.947	24.8
7	213	1.834	49.689	23.96	1.835	49.620	32.3
8	004	1.715	53.367	16.43	1.720	53.195	113.5

There was high consistency between the data of synthesized HAP and standard data base of HAP, with d-spacing values and peak intensity matches that of stoichiometric HAP (Reference code: 01-086-0740). No other impurity peaks is observed in the XRD pattern, which indicates the chief inorganic phase of the HAP sample. The stability of the HAP depends on the pH value of the reacting suspension. For a precipitated suspension, the stability will be poor when pH value is below 10.30, and so to maintain a stable suspension a reaction in which the pH is higher than 10.30 is required at room temperature. For chemical stability reasons, the higher pH values are utilized in HAP synthesis. Here between synthesized HAP has high consistency with standard HAP powder (Ref. Pattern: Hydroxyapatite, 01-086-0740) because the pH value of synthesized HAP was 11. The stable phase of HAP was hexagonal di-pyramidal at room temperatures.

When the sample is heated from 100˚C, 450˚C, 900˚C, up to 1200˚C (1 h holding time), further nucleation/growth of the hexagonal di-pyramidal nanocrystals occurs inside the synthesized HAP particles. Above 1200˚C, the decomposition of HAP partly into tricalcium phosphate was reported by Raynaud *et al*.

3.1.2. XRD Analysis of HAP/f-MWCNTs/Cobalt Ferrites Composites

The XRD pattern of cobalt ferrites oxide powders were shown in Figure 3(a) in which all the diffraction peaks were derived to the face-centred cubic structure of cobalt ferrite without other crystalline impurity peaks.

The sample was shown the reflection planes of (111), (220), (222), (311), (400), (422), (511), and (440), which confirms the presence of cobalt ferrites with a face-centred cubic structure [27]. These obtained XRD peaks have high consistency with the data obtained from the Joint Committee on powder Diffraction standards (JCPDS). The low diffraction peaks at 26.1˚ and 48.6˚ were assigned to graphite (002) and (100) planes of f-MWCNTs. Other peaks at 44.1˚ and 54.6˚ are assigned to (111) and (004) reflections of f-MWCNTs. The remaining peaks at 26.1˚, 28.2˚, 29.3˚, 32.5˚, 33˚, 34.5˚, 40˚, 47˚ 49.7˚, and 53.3˚ were assigned to (002), (102), (210), (211), (300), (202), (310), (222), (312), (213), and (004) planes of synthesized HAP respectively (JCPDS PDF No. 09-0432). It was found that the intensity of graphite peak (002) increased with sintering temperature which implies that more graphite structure is developed at higher temperature. No other peaks corresponding to CaP (Calcium phosphate) between 30˚ and 31˚ are detected at all sintering temperature, which was governed that the reaction resulted in the formation of phase pure HAP. Here in Figure 3. XRD pattern of

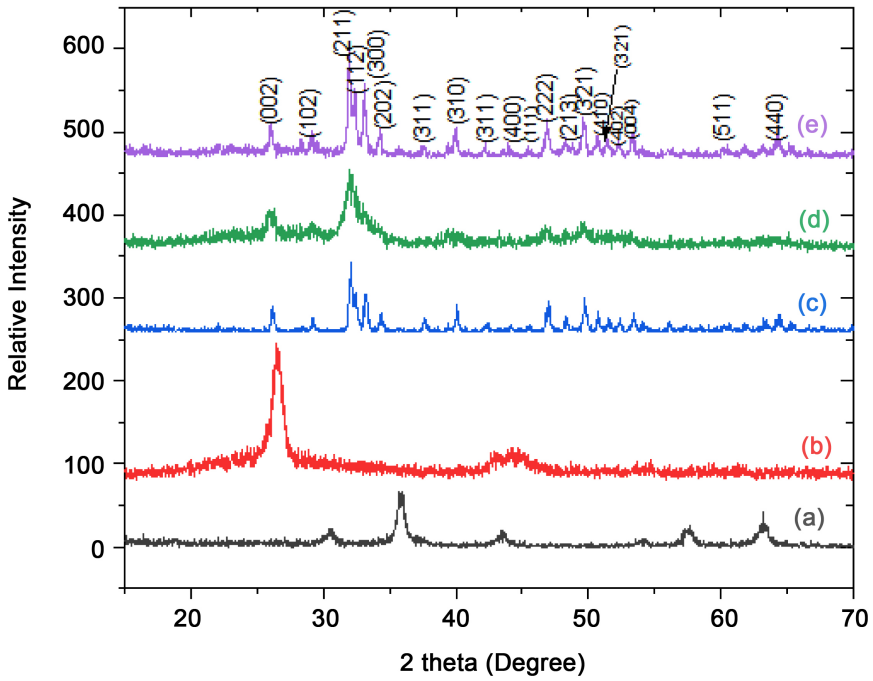

Figure 3. XRD pattern of (a) cobalt ferrites oxide ($CoFe_2O_4$) (b) f-MWCNTs (c) pure HAP (d) HAP/f-MWCNTs (e) HAP/f-MWCNTs/Cobalt ferrite composite.

(a) cobalt ferrite oxide ($CoFe_2O_4$) (b) f-MWCNTs (c) pure HAP (d) HAP/f-MWCNTs were sintered at room temperature but the final HAP/f-MWCNTs/Cobalt ferrite composites were sintered at 800˚C, because at 800˚C all peaks were governed. It was seen that crystalline peaks of the HAP/f-MWCNTs/Cobalt ferrite composite in **Figure 3(e)** were sharper than pure HAP, f-MWCNTs and Cobalt ferrite which was indicated that crystalline phases of HAPand Cobaltferrite on f-MWCNTs sidewall possessed high crystallizable. Because of the coinciding of (002) reflection of HAP, the typical (002) diffraction of f-MWCNTs is not distinctly observed for HAP /f-MWCNTs/Cobalt ferrite composite.

3.2. FT-IR Analysis

3.2.1. FTIR Absorption Studies of Sample HAP

FTIR investigation of HAP sample was shown in **Figure 4**. Broad size bands appearing at wave number values of 876, and 1442 cm^{-1} are indicative of the carbonate ion substitution [28]. The materials synthesized at lower temperatures show more absorption intensities indicating more impurity due to water molecules. The characteristic absorption bands for PO_4^{3-} appear at 564, 612, and 1064 cm^{-1}. The absorption peak at 1064 cm^{-1} ($\vartheta 3$ band) was very strong and the peak 612 cm^{-1} ($\vartheta 2$ band) was medium. The bands at 900 - 1200 cm^{-1} were the starching mode of PO_4^{3-} group.

The sharp peaks at 564 cm^{-1} ($\vartheta 4$ band) and 612 cm^{-1} correspond to bending vibration of PO_4^{3-} in hydroxyapatite. FTIR study of synthesized HAP were similar to those reported by Aili Wang *et al.* [29]; Murugan R *et al.* [30]; and Nejati E *et al.* [31].

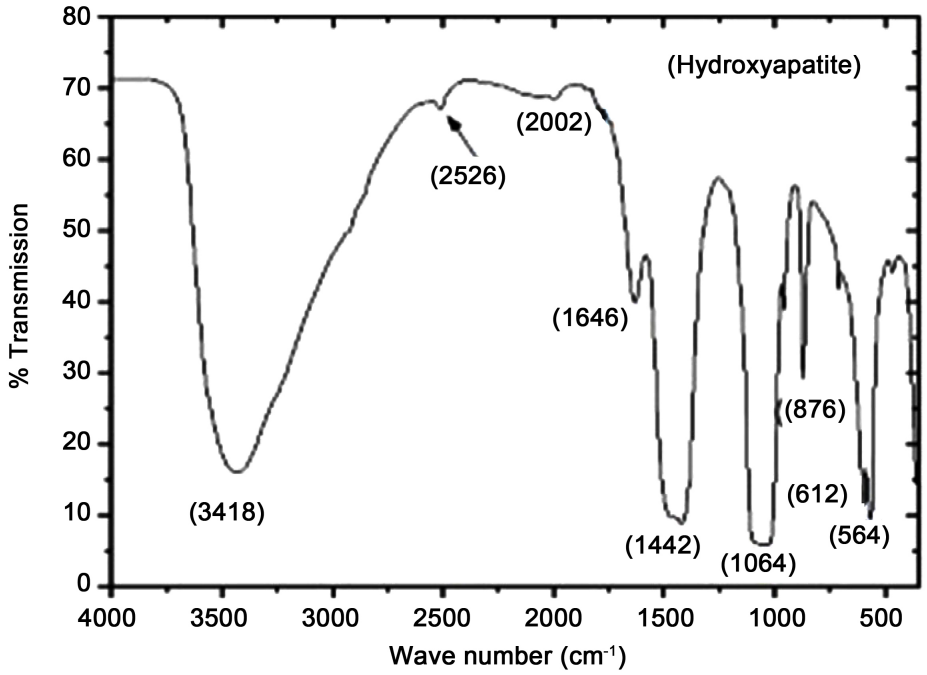

Figure 4. FTIR spectrum of HAP powder.

3.2.2. FTIR Absorption Studies of HAP/f-MWCNTs/Ferrites Composites

FTIR spectra of the HAP/f-MWCNTs/cobalt ferrites composites in the range 400 - 4000 cm^{-1} were shown in **Figure 5**. The FTIR spectrum were confirmed at bands corresponding to PO_4^{3-} ($\vartheta 3$ – 1050, $\vartheta 2$ – 980, $\vartheta 4$ – 610, $\vartheta 4$ – 576 cm^{-1}) and CO_3^{2-} ($\vartheta 3$ – 1428, $\vartheta 2$ –870 cm^{-1}) respectively [32]. The broad band at 3446 cm^{-1} is ascribed due to the O-H stretch of the hydroxyl group which can be qualified to the oscillation of carboxyl groups (O=C-OH and C-OH) [33]. The peak found at 1640 cm^{-1} is due to C=C stretching of the f-MWCNTs [34].

The prominent peak at 1050 cm^{-1} is associated with O-H stretch from strongly hydrogen bonded –COOH. The carbonate containing HAP was chemically and mechanically more similar to that in natural anisotropic bone. The spectrum in the $\vartheta 4$ PO_4^{3-} dominion exhibits the bands at 610 and 576 cm^{-1} is allotted to PO_4^{3-} ions in apatite sites. In the $\vartheta 2$ CO_3^{2-} field exhibits the band at 870 cm^{-1} which may improve the bioactivity of HAP and similar characteristic ones observed in bone crystals. The FTIR spectrum were confirmed at bands corresponding to PO_4^{3-} ($\vartheta 3$ –1098, $\vartheta 2$ – 984, $\vartheta 4$ – 614, $\vartheta 4$ – 568 cm^{-1}) and CO_3^{2-} ($\vartheta 3$ – 1450, $\vartheta 2$ – 860 cm^{-1}) respectively. Cobalt ferrite structure consists of two IR absorption bands, one at around 400 cm^{-1} which attributes to stretching vibration of tetrahedral groups $Fe^{3+}O^{2-}$ and other at around 600 cm^{-1} representing octahedral group complex $Co^{2+}O^{2-}$ [35] [36]. In the present investigation the above said bands appear at around 360 and 568 cm^{-1} respectively, which confirms the formation of $CoFe_2O_4$. So, it is governing that our synthesized composites contain f-MWCNTs and cobalt ferrite with HAP.

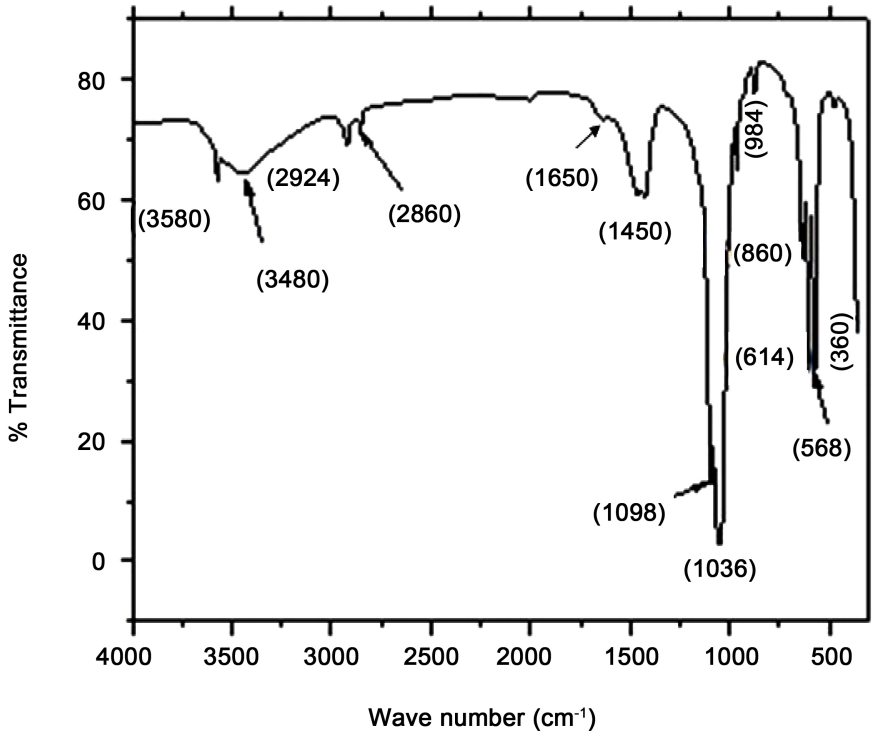

Figure 5. FTIR spectra of HAP/f-MWCNTs/cobalt ferrite composites.

3.3. Analysis of Electrical Properties (Frequency Dependent Resistivity)

The resistivity of the HAP/x wt.% f-MWCNTs/ y wt.% $CoFe_2O_4$ composites were shown in Figure 6 and Figure 7 (where x = 1, 3, 5 and y = 1, 3, 5) sintered at 800˚C for 1 hour as function of frequency. In this investigation ac resistivity of HAP/f-MWCNTs/$CoFe_2O_4$ composites were slightly changed with the increase of x content and rapidly changed with the increase of y content.

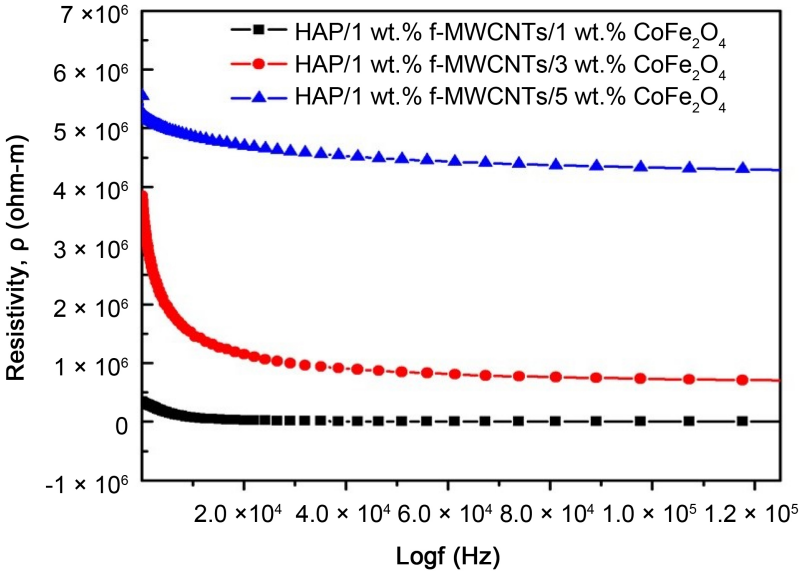

Figure 6. Variation of AC resistivity for (HAP/1 wt.% f-MWCNTs)/1 wt.% $CoFe_2O_4$, (HAP/1 wt.% f-MWCNTs)/3 wt.% $CoFe_2O_4$, (HAP/1 wt.% f-MWCNTs)/5 wt.% $CoFe_2O_4$ composites sintered at 800˚C.

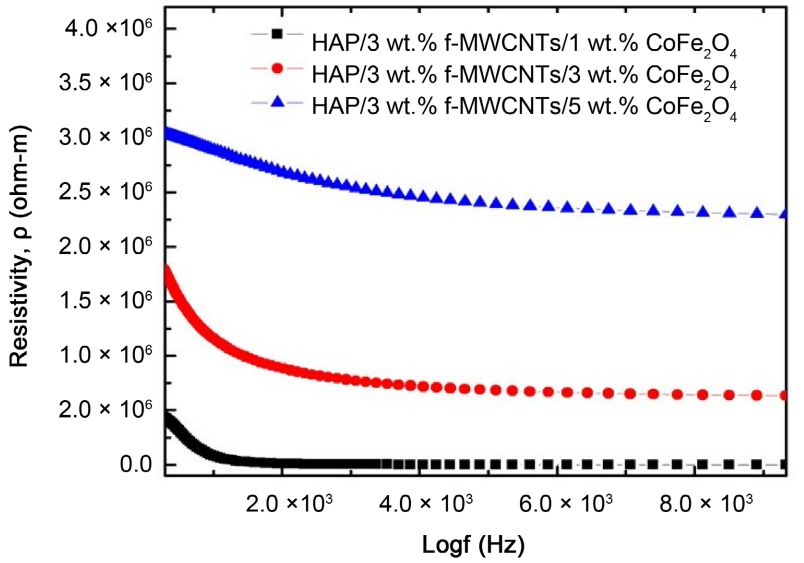

Figure 7. Variation of AC resistivity for (HAP/3 wt.% f-MWCNTs)/1 wt.% $CoFe_2O_4$, (HAP/3 wt.% f-MWCNTs)/3 wt.% $CoFe_2O_4$, (HAP/3 wt.% f-MWCNTs)/5 wt.% $CoFe_2O_4$ composites sintered at 800˚C.

The increase in frequency improves the hopping the frequency of charge carries resulting in an increase in the conduction process thereby decrease the resistivity. The minimum resistivity occurred when the frequency of the hopping charge carries was equal to the applied field frequency termed as resonance frequency jumped *i.e*., the jumping frequency of hopping charge carries were almost equal to that of the applied Ac electric field. With the increase in frequency, the resistivity increased most linearly which could be due to the retardation of hopping charge carries with increasing applied field frequency. From the investigation, we observed a rapid dispersion at lower frequency region. The decrease of resistivity that means increase of conductivity could be due to the absence of dispersion in permittivity at higher frequency. Figure 6 and Figure 7 also implied that (HAP/1 wt.% f-MWCNTs)/5 wt.% $CoFe_2O_4$, and (HAP/3 wt.% f-MWCNTs)/5 wt.% $CoFe_2O_4$ composites were higher conductivity, corresponding lower resistivity than all other composites.

3.4. Analysis of VSM Data (Hysteresis Curve)

Magnetization (M) versus applied magnetic field (H) plots for synthesis HAP/F-MWCNTs and HAP/F-MWCNTs/$CoFe_2O_4$ composites were presented in Figure 8 which were investigated below. The Vibrating-sample magnetometer (VSM) analysis were carried out at room temperature in plane and out of plane configurations with a maximum field of 11K Oe, in steps of 5 Oe. Normally pure HAP do not contain any magnetic property. But when any incorporation of magnetic materials occurred with HAP, its magnetic property increased significantly which was seen from the Figure 8(d) that the curve was not saturated

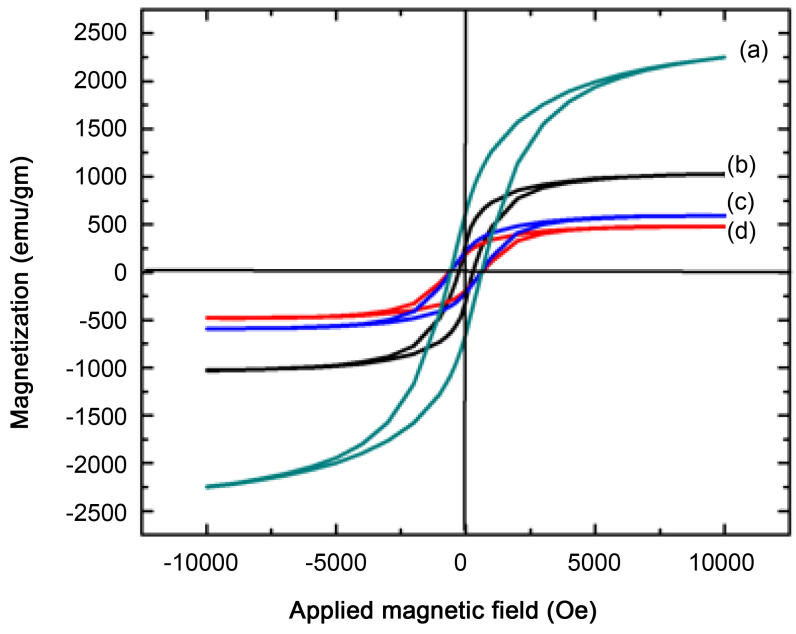

Figure 8. Hysteresis curve of (a) (HAP/3 wt.% f-MWCNTs)/5 wt.% $CoFe_2O_4$, (b) (HAP/3 wt.% f-MWCNTs)/3 wt.% $CoFe_2O_4$, (c) (HAP/3 wt.% f-MWCNTs)/1 wt.% $CoFe_2O_4$) (d) (HAP/3 wt.% f-MWCNTs) composites.

Table 2. Magnetic properties obtained from VSM measurements.

Sample	Coercivity Hc (Oe)	Magnetization Ms (emu/g)	Remanence Mr (emu/g)	Squareness Mr/Ms
HAP/3% f-MWCNTS	410.30	50	20	0.4
(HAP/3% f-MWCNTs)/1% cobalt ferrite	540.35	1500	650	0.433
(HAP/3% f-MWCNTs)/3% cobalt ferrite	630.15	2100	350.15	0.166
(HAP/3% f-MWCNTs)/5% cobalt ferrite	850.50	2400	650.45	0.27

perfectly and showed narrow hysteresis loop, which investigated that HAP/3 wt.% f-MWCNTs composites were poor magnetic material. When 1% of $CoFe_2O_3$ was added to the HAP/3 wt.% f-MWCNTs composites (**Figure 8(c)**), the hysteresis curve of this composites differed from hysteresis curve of HAP/3 wt.% f-MWCNTs, which exhibited more magnetic property. From **Figure 8** observed that magnetization, coercivity increased with the increase of f-MWCNTs and $CoFe_2O_4$. N. Kumar and K. Kumarobserved the squareness ratio of pure $CoFe_2O_4$ is 0.54 at room temperature and which was decreased to 0.47 with the increase of bismuth ion concentration [37].

The result was revealed that the hysteresis curve of (HAP/3 wt.% f-MWCNTs)/5 wt.% $CoFe_2O_4$ composites were given large hysteresis loop after adding f-MWCNTs and $CoFe_2O_4$.

It was mentioned that HAP was non-magnetic. Our present research revealed that the synthesized HAP could be imparted with magnetic properties by incorporating the phase reinforcements, like f-MWCNTs and cobalt ferrite. **Figure 8** showed hysteresis curve of (a) (HAP/3 wt.% f-MWCNTs)/5 wt.% $CoFe_2O_3$, (b) (HAP/3 wt.% f-MWCNTs)/3 wt.% $CoFe_2O_3$, (c) (HAP/3 wt.% f-MWCNTs)/1 wt.% $CoFe_2O_3$,) (d) (HAP/3 wt.% f-MWCNTs) composites. The Coercivity Hc (Oe), Magnetization, Ms (emu/g), Remanance, Mr (emu/g) and Squareness, Mr/Ms were obtained from magnetic hysteresis curve (**Table 2**).

We showed that coercivity of (HAP/3 wt.% f-MWCNTs)/5 wt.% $CoFe_2O_4$ composites were 850.50 Oe with magnetization 2400 emu/g, which implied that (HAP/3 wt.% f-MWCNTs)/5 wt.% $CoFe_2O_4$ composites were highly magnetic materials.

4. Conclusion

HAP/f-MWCNTs composites have been better bio-compatibility, higher mechanical property and even definite magnetism and wave-absorbing property.

For increasing electronic, magnetic and catalytic properties of the CNTs/HAP composites, we added a certain number of ferrites in this composite. The aim of the current research is to synthesis nano-sized high-quality HAP/f-MWCNTs/Cobalt ferrite composites and to carry out its characterization for electric and magnetic properties. The synthesized HAP/f-MWCNTs/Cobalt ferrite composites were sintered at a temperature of 800˚C to improve its crystallinity. For the sake of comprehensive study of these composites, detailed investigation was done by using advanced techniques like FT-IR, XRD, VSM and Impedance Analyser. It was seen that crystalline peaks of the HAP/f-MWCNTs/ cobalt ferrite composites were sharper than pure HAP, f-MWCNTs and cobalt ferrite which indicated that crystalline phases of synthesized HAP and cobalt ferrite on f-MWCNTs sidewall possessed high crystallizable. Because of the coinciding of (002) reflection of HAP, the typical (002) diffraction of f-MWCNTs was not distinctly observed for HAP/f-MWCNTs/ferrite composites, which exhibited that HAP had decomposed with f-MWCNTs. From FT-IR analysis, it was confirmed that the absorption bands of synthesized HAP which were similar to the standard HAP. For FT-IR analysis, there was carboxyl functional group formed on MWCNTs treated with nitric acid for 6 hours. The functional group of MWCNTs and cobalt-ferrite were present in the final composites. The electrical properties such as conductivity and resistivity of (HAP/x wt.% f-MWCNTs)/y wt.% $CoFe_2O_4$ composites (where x = 1, 3, 5 and y = 1, 3, 5) sintered at 800˚C for 1 hour were performed by impedance analyser. Ac resistivity of (HAP/x wt.% f-MWCNTs)/y wt.% $CoFe_2O_4$ composites (where x = 1, 3, 5 and y = 1, 3, 5) was slightly changed with the increase of x content and rapidly changed with the increase of y content. At low frequency the conductivity is approximate to zero and starts increasing at higher frequency. Conductivity shows the opposite trends of resistivity at frequency. The ac resistivity of (HAP/3 wt.% f-MWCNTs)/3 wt.% $CoFe_2O_4$ composites were very low, *i.e.*, its conductivity was significantly increased with frequency than all other composites. So, it was concluded that our synthesized composite was a good candidate for electrical applications. VSM data showed that coercivity of (HAP/3 wt.% f-MWCNTs)/5 wt.% $CoFe_2O_4$ composites were 850.50 Oe with magnetization 2400 emu/g, which implied that (HAP/3 wt.% f-MWCNTs)/5 wt.% $CoFe_2O_4$ composites were highly magnetic materials.

Conflicts of Interest

The authors declare no conflicts of interest.

References

[1] Ferraz, M.P., Monteiro, F.J. and Manuel, C.M. (2004) Hydroxyapatite Nanoparticles: A Review of Preparation Methodologies. *Journal of Applied Biomaterials and Biomechanics*, **2**, 74-80.

[2] Yusuf, P.S.M., Dahlan, K. and Witarto, A.B. (2010) Application of Hydroxyapatite in Protein Purification. *Makara Journal of Science*, **13**, 134-140.

https://doi.org/10.7454/mss.v13i2.413

[3] Kano, S., Yamazaki, A., Otsuka, R., Ohgaki, M., Akao, M. and Aoki, H. (1994) Application of Hydroxyapatite-Sol as Drug Carrier. *Bio-Medical Materials and Engineering*, **4**, 283-290. https://doi.org/10.3233/BME-1994-4404

[4] Kundu, B., Sinha, M.K., Mitra, M.K. and Basu, D. (2004) Fabrication and Characterization of Porous Hydroxyapatite Ocular Implant Followed by *Anin Vivo* Study in Dogs. *Bulletin of Materials Science*, **27**, 133-140. https://doi.org/10.1007/BF02708495

[5] Rajesh, R., Hariharasubramanian, A. and Ravichandran, Y.D. (2012) Chicken Bone as a Bioresource for the Bioceramic (Hydroxyapatite). *Phosphorus, Sulfur, and Silicon and the Related Elements*, **187**, 914-925. https://doi.org/10.1080/10426507.2011.650806

[6] Panneerselvam, R., Anandhan, N., Sivakumar, G., Ganesan, K.P., Marimuthu, T. and Sugumar, V. (2019) Role of Annealing Temperatures on Mechanical, Optical, Electrical and Magnetic Properties of Nanohydroxyapatite Biomaterial. *Journal of Nanoscience and Nanotechnology*, **19**, 4366-4376. https://doi.org/10.1166/jnn.2019.16364

[7] Iijima, S. and Ichihashi, T. (1993) Single-Shell Carbon Nanotubes of 1-NM Diameter. *Nature*, **363**, 603-605. https://doi.org/10.1038/363603a0

[8] Iijima, S. (1991) Helical Microtubules of Graphitic Carbon. *Nature*, **354**, 56-58. https://doi.org/10.1038/354056a0

[9] Khabashesku, V.N., Margrave, J.L. and Barrera, E.V. (2005) Functionalized Carbon Nanotubes and Nanodiamonds for Engineering and Biomedical Applications. *Diamond and Related Materials*, **14**, 859-866. https://doi.org/10.1016/j.diamond.2004.11.006

[10] Baviskar, D.T., Tamkhane, C.M., Maniyar, A.H. and Jain, D.K. (2012) Carbon Nanotubes: An Emerging Drug Delivery Tool in Nanotechnology. *International Journal of Pharmacy and Pharmaceutical Sciences*, **4**, 11-15.

[11] Balázsi, C., Kónya, Z., Wéber, F., Biró, L.P. and Arató, P. (2003) Preparation and Characterization of Carbon Nanotube Reinforced Silicon Nitride Composites. *Materials Science and Engineering: C*, **23**, 1133-1137. https://doi.org/10.1016/j.msec.2003.09.085

[12] Lupo, F., Kamalakaran, R., Scheu, C., Grobert, N. and Rühle, M. (2004) Microstructural Investigations on Zirconium Oxide-Carbon Nanotube Composites Synthesized by Hydrothermal Crystallization. *Carbon*, **42**, 1995-1999. https://doi.org/10.1016/j.carbon.2004.03.037

[13] Rul, S., Lefèvre-Schlick, F., Capria, E., Laurent, C. and Peigney, A. (2004) Percolation of Single-Walled Carbon Nanotubes in Ceramic Matrix Nanocomposites. *Acta Materialia*, **52**, 1061-1067. https://doi.org/10.1016/j.actamat.2003.10.038

[14] Li, A., Sun, K., Dong, W. and Zhao, D. (2007) Mechanical Properties, Microstructure and Histocompatibility of MWCNTs/HAp Biocomposites. *Materials Letters*, **61**, 1839-1844. https://doi.org/10.1016/j.matlet.2006.07.159

[15] Zhang, Y., Bai, Y. and Yan, B. (2010) Functionalized Carbon Nanotubes for Potential Medicinal Applications. *Drug Discovery Today*, **15**, 428-435. https://doi.org/10.1016/j.drudis.2010.04.005

[16] Tadic, D., Peters, F. and Epple, M. (2002) Continuous Synthesis of Amorphous Carbonated Apatites. *Biomaterials*, **23**, 2553-2559. https://doi.org/10.1016/S0142-9612(01)00390-8

[17] Zakharov, N.A., Polunina, I.A., Polunin, K.E., Rakitina, N.M., Kochetkova, E.I., Sokolova, N.P. and Kalinnikov, V.T. (2004) Calcium Hydroxyapatite for Medical Applications. *Inorganic Materials*, **40**, 641-648. https://doi.org/10.1023/B:INMA.0000032000.83171.9f

[18] Fan, H.-M., Yi, J.-B., Yang, Y., Kho, K.-W., Tan, H.-R., Shen, Z-X., Ding, J., Sun, X.-W., Olivo, M.C. and Feng, Y.-P. (2009) Single-Crystalline MFe_2O_4 Nanotubes/Nanorings Synthesized by Thermal Transformation Process for Biological Applications. *ACS Nano*, **3**, 2798-2808. https://doi.org/10.1021/nn9006797

[19] Srinivasan, S.Y., Paknikar, K.M., Bodas, D. and Gajbhiye, V. (2018) Applications of Cobalt Ferrite Nanoparticles in Biomedical Nanotechnology. *Nanomedicine*, **13**, 1221-1238. https://doi.org/10.2217/nnm-2017-0379

[20] Nongjai, R., Khan, S., Asokan, K., Ahmed, H. and Khan, I. (2012) Magnetic and Electrical Properties of in Doped Cobalt Ferrite Nanoparticles. *Journal of Applied Physics*, **112**, Article ID: 084321. https://doi.org/10.1063/1.4759436

[21] Sugimoto, M. (2004) The Past, Present, and Future of Ferrites. *Journal of the American Ceramic Society*, **82**, 269-280. https://doi.org/10.1111/j.1551-2916.1999.tb20058.x

[22] Alivisatos, A.P. (1996) Semiconductor Clusters, Nanocrystals, and Quantum Dots. *Science*, **271**, 933-937. https://doi.org/10.1126/science.271.5251.933

[23] Mukherjeea, M., Kundub, B., Sen, S. and Chandad, A. (2014) Improved Properties of Hydroxyapatite-Carbon Nanotube Biocomposite: Mechanical, *in Vitro* Bioactivity and Biological Studies. *Ceramics International*, **40**, 5635-5643. https://doi.org/10.1016/j.ceramint.2013.10.158

[24] Koziol, K., Boskovic, B.O. and Yahya, N. (2010) Synthesis of Carbon Nanostructures by CVD Method. In: *Carbon and Oxide Nanostructures. Advanced Structured Materials*, Vol. 5, Springer, Berlin, 23-49. https://doi.org/10.1007/8611_2010_12

[25] Zhao, L., Zhang, H., Xing, Y., Song, S., Yu, S., Shi, W., Guo, X., Yang, J., Lei, Y. and Cao, F. (2008) Studies on the Magnetism of Cobalt Ferrite Nanocrystals Synthesized by Hydrothermal Method. *Journal of Solid State Chemistry*, **181**, 245-252, https://doi.org/10.1016/j.jssc.2007.10.034

[26] Montoro, L.A. and Rosolen, J.M. (2006) A Multi-Step Treatment to Effective Purification of Single-Walled Carbon Nanotubes. *Carbon*, **44**, 3293-3301. https://doi.org/10.1016/j.carbon.2006.06.018

[27] Swain, S.K. and Sarkar, D. (2011) A Comparative Study: Hydroxyapatite Spherical Nanopowders and Elongated Nanorods. *Ceramics International*, **37**, 2927-2930. https://doi.org/10.1016/j.ceramint.2011.03.077

[28] Abden, M.J., Afroze, J.D., Alam, M.S. and Bahadur, N.M. (2016) Pressureless Sintering and Mechanical Properties of Hydroxyapatite/functionalized Multi-Walled Carbon Nanotube Composite. *Materials Science and Engineering*: *C*, **67**, 418-424. https://doi.org/10.1016/j.msec.2016.05.018

[29] Wang, A., Liu, D., Yin, H., Wu, H., Wada, Y., Ren, M., Jiang, T., Cheng, X. and Xu, Y. (2007) Size-Controlled Synthesis of Hydroxyapatite Nanorods by Chemical Precipitation in the Presence of Organic Modifiers. *Materials Science and Engineering*: *C*, **27**, 865-869. https://doi.org/10.1016/j.msec.2006.10.001

[30] Murugan, R. and Ramakrishna, S. (2004) Bioresorbable Composite Bone Paste Using Polysaccharide Based Nano Hydroxyapatite. *Biomaterials*, **25**, 3829-3835. https://doi.org/10.1016/j.biomaterials.2003.10.016

[31] Nejati, E., Firouzdor, V., Eslaminejad, M.B. and Bagheri, F. (2009) Needle-Like Nano Hydroxyapatite/Poly(L-Lactide Acid) Composite Scaffold for Bone Tissue

Engineering Application. *Materials Science and Engineering*: *C*, **29**, 942-949. https://doi.org/10.1016/j.msec.2008.07.038

[32] Han, J.-K., Song, H.-Y., Saito, F. and Lee, B.-T. (2006) Synthesis of High Purity Nano-Sized Hydroxyapatite Powder by Microwave-Hydrothermal Method. *Materials Chemistry and Physics*, **99**, 235-239. https://doi.org/10.1016/j.matchemphys.2005.10.017

[33] Davis, W.M., Erickson, C.L., Johnston, C.T., Delfino, J.J. and Porter, J.E. (1999) Quantitative Fourier Transform Infrared Spectroscopic Investigation Humic Substance Functional Group Composition. *Chemosphere*, **38**, 2913-2928. https://doi.org/10.1016/S0045-6535(98)00486-X

[34] Abdullah, M.P. and Zulkepli, S.A. (2015) The Functionalization and Characterization of Multi-Walled Carbon Nanotubes (MWCNTs). *AIP Conference Proceedings*, **1678**, Article ID: 050033. https://doi.org/10.1063/1.4931312

[35] Waldron, R.D. (1955) Infrared Spectra of Ferrites. *Physical Reviews*, **99**, 1727-1735. https://doi.org/10.1103/PhysRev.99.1727

[36] Kumbhar, V.S., Jagadale, A.D., Shinde, N.M. and Lokhande, C.D. (2012) Chemical Synthesis of Spinel Cobalt Ferrite ($CoFe_2O_4$) Nano-Flakes for Supercapacitor Application. *Applied Surface Science*, **259**, 39-43. https://doi.org/10.1016/j.apsusc.2012.06.034

[37] Kumar, N.S. and Kumar, K.V. (2016) Effect of Bi3+ Ion Substitution on Magnetic Properties of Cobalt Nano Ferrites Prepared by Sol-Gel Combustion Method. *Soft Nanoscience Letters*, **6**, 37-44. https://doi.org/10.4236/snl.2016.63004